Biosensors and Bioelectronics 191 (2021) 113420

Contents lists available at ScienceDirect

Biosensors and Bioelectronics

journal homepage: www.elsevier.com/locate/bios

# Franz cells for facile biosensor evaluation: A case of HRP/SWCNT-based hydrogen peroxide detection via amperometric and wireless modes

Van Chinh Hoang [a,b,c], Atefeh Shafaat [a,b], Skaidre Jankovskaja [a,b], Vincent G. Gomes [c,**], Tautgirdas Ruzgas [a,b,*]

[a] Department of Biomedical Science, Faculty of Health and Society, Malmö University, SE-205 06, Malmö, Sweden
[b] Biofilms - Research Center for Biointerfaces, Malmö University, SE-205 06, Malmö, Sweden
[c] The University of Sydney, School of Chemical and Biomolecular Engineering, NSW, 2006, Australia

ARTICLE INFO

*Keywords:*
Hydrogen peroxide biosensor
Epidermal sensing
Skin membrane
Franz cell

ABSTRACT

Reducing animal use in biosensor research requires broader use of *in vitro* methods. In this work, we present a novel application of Franz cells suitable for biosensor development and evaluation *in vitro*. The work describes how Franz cell can be equipped with electrodes enabling characterization of biosensors in close proximity to skin. As an example of a sensor, hydrogen peroxide biosensor was prepared based on horseradish peroxidase (HRP)/single-walled carbon nanotube (SWCNT)-modified textile. The electrode exhibited lower detection limit of 0.3 μM and sensitivity of 184 μA $mM^{-1}$ $cm^{-2}$. The ability of this biosensor to monitor $H_2O_2$ penetration through skin and dialysis membranes was evaluated in Franz cell setup in amperometric and wireless modes. The results also show that catalase activity present in skin is a considerable problem for epidermal sensing of $H_2O_2$. This work highlights opportunities and obstacles that can be addressed by assessment of biosensors in Franz cell setup before progressing to their testing in animals and humans.

## 1. Introduction

It is estimated that more than 192 million animals were used in biomedical research in 2015, which show 36.9% increase since 2005 (Taylor and Alvarez, 2019). The statistics about animal use in biosensor research is not available, but a decreasing number is not expected. To the contrary, broad use of animals and humans can be seen in exploding research on wearables (Ray et al., 2019; Salim and Lim, 2019; Stoppa and Chiolerio, 2014), smart textiles (Park and Jayaraman, 2003), wireless biosensors (Stuart et al., 2021), epidermal electronics and epidermal sensing (Heikenfeld, 2016; Ray et al., 2019; Wang et al., 2018; Xu et al., 2019). The situation with animal use is not surprising since high number of biosensors and biosensor-driven drug delivery systems (Keum et al., 2020) are being designed to function in intimate contact with biological barriers such as the skin (Heikenfeld et al., 2018) or cornea (Stuart et al., 2021).

It is easy to note that development of wearable and epidermal biosensors has considerable similarity to the design and application of topical and transdermal drug delivery systems. Both research fields aim to benefit from deeper knowledge of skin structure and describe biomarker or bioactive flux by accounting for their partition and diffusion in skin (Heikenfeld et al., 2018; Mitragotri, 2003; Ullah et al., 2018), and even exploit iontophoresis to make biosensing or drug delivery more controllable, reproducible and quicker (Guy et al., 2000; Ventura et al., 2017). The research field of transdermal drug delivery, however, has been, far early, experiencing high demand to reduce animal tests. To solve the problem, the development of topical and transdermal drug delivery systems systematically introduced appropriate *in vitro* tests (Junqueira Garcia et al., 2018). By the same logic, to reduce the use of animals for testing biosensors, should be of high relevance in the research field of biosensors and bioelectronics. In this context, the use of *in vitro* systems, which are well-accepted in the development of topical and transdermal drug delivery, could be more broadly considered in biosensor research.

The introduction of Franz cells for the development of transdermal and topical drug delivery has revolutionized this field of research (Bartosova and Bajgar, 2012; Raney et al., 2008). The setup (Fig. 1) is very simple and it comprises two compartments, which are separated by

* Corresponding author. Biofilms - Research Center for Biointerfaces, Malmö University, SE-205 06, Malmö, Sweden.
** Corresponding author.
*E-mail addresses:* vincent.gomes@sydney.edu.au (V.G. Gomes), tautgirdas.ruzgas@mau.se (T. Ruzgas).

https://doi.org/10.1016/j.bios.2021.113420
Received 26 December 2020; Received in revised form 1 June 2021; Accepted 5 June 2021
Available online 18 June 2021

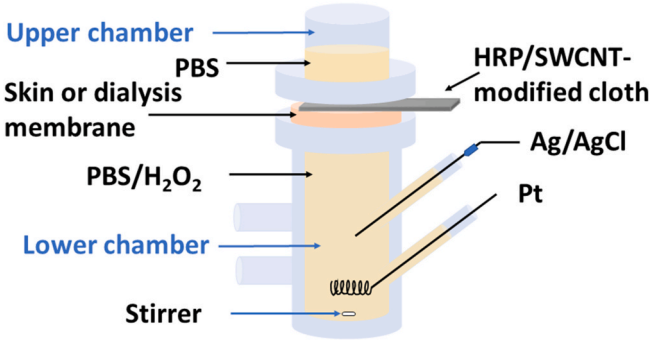


**Fig. 1.** Franz cell equipped with a biosensor (HRP/SWCNT-modified cloth) for amperometric measurements of $H_2O_2$. Skin membrane (skin's dermal side face lower chamber) or its surrogate, dialysis membrane, is placed between the upper and the lower chambers of the Franz cell. The picture demonstrates one of the convenient and simplest placements of the electrodes in the cell enabling performance of electrochemical biosensor. To model ROS production in the skin, $H_2O_2$ was injected into the lower chamber of the cell. The aim of this experimental setup was to demonstrate that the biosensor in Franz cell (in the proposed three electrode placement and connection) is able to detect $H_2O_2$, which penetrates the skin membrane or its surrogate.

a membrane. Real biological membranes, e.g., skin, can be collected from animals slotted for food or from human surgical wastes. Complete avoidance of animal and human material is also attempted by using 3D epidermal skin equivalents produced by cultivation of keratinocytes, solely, or with the presence of other cell types (Niehues et al., 2018; van den Bogaard et al., 2021). In a Franz cell based experiment, the drug formulation is usually added into the upper chamber and its concentration in the lower chamber is monitored in due time by sampling of approximately 0.2 mL solution followed by chromatographic analysis.

To the best of our knowledge, the Franz cell setup is yet to be adopted for testing biosensors and bioelectronic devices. However, it is intuitive that non-invasive biosensing and functioning of epidermal bioelectronics, e.g., biofuel cells on skin, often rely on diffusion of different compounds from viable tissues to the surface of the skin (Bandodkar et al., 2015) - the direction opposite to the diffusion of compounds in transdermal drug delivery. This suggests that the optimization of biosensor-skin interface and biosensor characterization should benefit from their tests in Franz cells. Additionally, plenty of relevant knowledge can also be exploited, such as, identification and description of permeability pathways of relevant metabolites (Jankovskaja et al., 2020; Mitragotri, 2003). A number of possibilities to experimentally change environmental conditions, such as, skin temperature and hydration (Bjoerklund et al., 2013; Morin et al., 2020) and the assessment of their effects on the skin and on biosensor performance could be easier realized using Franz cell experiments than in real clinical settings.

The aim of this work was, thus, to demonstrate novel application of Franz cells for the development and testing of biosensors. As an example, an electrochemical biosensor for $H_2O_2$ detection based on HRP-modified conducting fabrics was chosen. The performance of this biosensor in Franz cell is demonstrated in amperometric as well as in wireless modes. The presented Franz cell – biosensor setup illustrates possible placement and connection of the electrodes as well as demonstrates experimental possibilities and obstacles for biosensor studied at skin membranes or its surrogate, dialysis membrane.

## 2. Materials and methods

### 2.1. Materials

Phosphate buffer saline (PBS) tablets, $HNO_3$, $AgNO_3$, KCl, ascorbic acid, sodium citrate, isopropanol, $H_2O_2$ (30%), beeswax (Cera alba), SWCNT (>85% carbon), diameter 1.3–2.3 nm, and HRP (Type VI, lyophilized powder, ≥250 units/mg solid) were purchased from Sigma Aldrich (Darmstadt, Germany). Screen printed electrodes, SPEs, with working Au electrode were purchased from Metrohm, Oviedo (Asturias), Spain. To model skin permeability which is practically possible only for compounds with molecular weight of less than 500 Da, a dialysis membrane (cellulose ester, molecular weight cut off 100–500 Da, diameter 15 mm) was purchased from Spectrum Labs (California, USA). Milli-Q (MQ) water with 18.2 MΩ cm resistivity was used throughout the study. A phosphate-buffered saline (PBS) solution containing 10 mM phosphate buffer, 2.7 mM KCl and 137 mM NaCl (pH = 7.4) was prepared from PBS tablets.

### 2.2. Fabrication of SWCNTs-cloth

Commercial cloth (50% Bomull, 50% Lin) was cleaned by ultrasonicating in ethanol/water mixture (1:1, v:v) for 1 h. After that, the textile was washed several times with MQ water and dried at 60 °C overnight. Finally, the textile was cut into small strips (1 cm × 3 cm) and used for modification aiming to produce flexible electrodes.

The chemically oxidized single-walled CNTs (SWCNTs) were prepared using concentrated nitric acid as described elsewhere (Goh et al., 2013). Briefly, SWCNTs were first purified by heating at 300 °C for 30 min in air. Purified SWCNTs (1 g) were treated by refluxing in 180 mL $HNO_3$ 65% at 80 °C for 8 h. After cooling to room temperature, the resultant suspension was diluted by 2 L MQ water. Subsequently, the solid was collected by filtration, washed by MQ water several times till neutral pH was obtained and finally dried at 60 °C overnight.

The slurry was prepared by tip-sonicating the SWCNTs in isopropanol/water mixture (9:1, v:v) (Branson Digital Sonifier 450, USA) for 30 min with 50% amplitude and 3 s on/3 s off pulse mode; resulted in 0.5 mg $mL^{-1}$ SWCNT suspension. Afterwards, 200 μL of the suspension was drop-casted onto the cloth (1 cm × 1 cm), followed by drying in air. To fabricate the current collector (i.e., conducting path for connecting to potentiostat), 80 μL of the suspension was drop-casted onto the side of cloth (0.2 cm × 2 cm) and a small amount of wax was coated to avoid its wettability (see Fig S1, Supporting Information). Finally, the SWCNT-modified cloth was immersed in an HRP solution (0.15 mg $mL^{-1}$) in $H_2O$ for 30 min in order to immobilize HRP enzyme by simple physical adsorption.

### 2.3. Material characterization

#### 2.3.1. Surface characterization

Surface morphology of the electrodes was investigated by a scanning electronic microscope (SEM, Zeiss) operating at 20 kV.

#### 2.3.2. Electrochemical characterization

The capacitive features of SWCNT-modified cloth were characterized by using an EmStat3 Blue potentiostat (PalmSens, Houten, The Netherlands) in three-electrode configuration in PBS electrolyte with SWCNT-modified cloth, Pt wire and Ag/AgCl as the working, counter and reference electrodes, respectively. Cyclic voltammetry (CV) was conducted in a potential window between −0.2 and 0.8 V (vs. Ag/AgCl). The specific capacitance ($C_{sp}$) of the materials was estimated by:

$$C_{sp} = \frac{1}{2 \cdot m \cdot V \cdot \nu} \int_{V_-}^{V_+} i(V) dV \quad (1)$$

where $i(V)$ and $\nu$ are the current measured during CV scan and potential scan rate, respectively; $V$ ($V = V_+ - V_-$) illustrates the potential range of the scan; $m$ is the mass of the active (SWCNT) materials (0.1 mg).

Open circuit potential (OCP) of the working electrodes was measured against Ag/AgCl reference electrode (both immersed in PBS) by using EmStat3 Blue potentiostat in constant current potentiometric mode. The $H_2O_2$ sensing with the textile electrode was conducted by

chronoamperometry. The resistance of electrodes was measured with a multimeter model EX542 (Extech Instruments, FLIR Systems, Inc., Waltham, MA). For wireless reading of the biosensor, the antenna of the biosensor was irradiated by electromagnetic (radio frequency) field and absorbed electromagnetic power (more specifically, the reflection characteristic S11) was measured by using a vector network analyzer DG8-SAQ VNA (SDR-Kits, Melksham, UK). In our case, VNA served as a reader of a passive near field communication (NFC) tag. The antenna of the wireless biosensor was based on a passive NFC tag (Smartrac, 13.56 MHz). To make a wireless biosensor the tag antenna was cut and reconnected by a silver nanoparticle (AgNP) layer placed on a screen-printed electrode. The AgNPs were simply drop-casted between the working and the counter electrodes of the SPE. This allowed to achieve wireless reading of biosensing redox reaction, i.e., oxidation of Ag to AgCl by $H_2O_2$ catalyzed by HRP.

### 2.4. Franz cell setup

Franz cell from PermeGear Inc. (Hellertown, PA) with opening diameter 0.9 cm and lower chamber volume of 6 mL (see Fig. 1) was used to demonstrate feasibility of the prepared biosensor to monitor $H_2O_2$ penetration through skin and its model, dialysis membrane. The porcine skin thickness was 500 μm. Porcine skin, prior to its usage for $H_2O_2$ permeation experiments, was exposed to UVB radiation to inhibit (bleach) catalase activity (for preparation of skin membranes see Supporting Information). Porcine skin membrane or its model, dialysis membrane, together with HRP/SWCNT-modified cloth positioned on top of the membrane, were mounted between the two chambers of the Franz cell (Fig. 1). Both lower and upper chambers of the Franz cell were filled with PBS (pH 7.4) solution, 6 mL and 0.2 mL, respectively. Then, porcine skin or dialysis membrane was left to equilibrate in the Franz cell for 30–60 min; until the amperometric current of the cloth based electrode reached stable baseline current. Next, $H_2O_2$ was added to the lower Franz cell chamber to reach concentration of 0.5 mM (in case of dialysis membrane) or 4 mM (in case of skin). The solution in the lower chamber was continuously stirred and the Franz cell was kept at room temperature throughout the experiment. The $H_2O_2$ penetration through the skin and dialysis membrane was monitored by recording the current chronoamperometrically or by electromagnetic field (radio frequency) reflection (S11 characteristic) from the biosensor coupled antenna (see Supplementary Information for more comprehensive explanation of wireless S11 measurement).

## 3. Results and discussion

To promote reduced animal use in biosensor and bioelectronics research, in this work, we introduce a novel application of Franz cells. Demonstration of the performance of a textile-based biosensor for $H_2O_2$ monitoring on skin or its surrogate, hosted in Franz cell, was chosen as an example. The fabric based biosensor is particularly relevant since flexible biosensors are often tested for sensing on skin or epidermal sensing (Heikenfeld, 2016; Ray et al., 2019; Stuart et al., 2021; Wang et al., 2018; Xu et al., 2019). Additionally, epidermal sensing of $H_2O_2$, which is one of the most stable reactive oxygen species (ROS), might be important in monitoring inflammatory skin disorders. For instance, it has been reported that $H_2O_2$ can reach 1 mM in the epidermis of patients affected by vitiligo (Schallreuter et al., 1999). Our experiments, thus, were directed to demonstrate a possibility and to assess obstacles for monitoring of similar $H_2O_2$ concentrations by biosensor functioning on porcine skin or on skin substitute (dialysis membrane) mounted in Franz cell. Fig. 1 presents a Franz cell equipped with an electrochemical biosensor for $H_2O_2$ detection. The stratum corneum side of skin membrane faces upper Franz cell chamber. The media in the lower chamber can be chosen to model reactions and concentrations which are expected in the viable tissue, i.e., dermal side of the skin. The drawing in Fig. 1 shows one of the simplest placements and connections of the electrodes without demanded printing of the electrodes on one substrate. In this work, working electrode was comprised of cotton fabrics modified with SWCNT and HRP. Ag/AgCl and Pt noted in Fig. 1, show a convenient placement of Ag/AgCl/$KCl_{sat}$ reference and Pt counter electrodes, respectively. In the Franz cells from PermeGear, the lower chamber must be filled with 6 mL solution; in these experiments we used PBS. The upper chamber hosts the working biosensor electrode. To ensure the wetting of the entire electrode by the electrolyte in contact with skin, the chamber was filled with 0.2 mL of the solution; 1.2 mL is maximum volume possible. To demonstrate biosensor performance in the Franz cell, the analyte, i.e., $H_2O_2$, was injected into the lower chamber and continuously mixed with a magnetic stirrer. It was expected that the analyte will diffuse through the skin membrane and will be detected by the biosensor. To realize the monitoring, the electrodes were connected to three-electrode potentiostate for amperometric measurement. The text below summarizes the main features of the biosensor and its characteristics.

### 3.1. Preparation and characterization of e-textile electrode based on SWCNT-modified cloth

To prepare textile based $H_2O_2$ biosensor, a cotton textile was modified with carbon nanotubes by drop-casting their suspension on the fabrics. The photo and morphology of the resulting textile electrode are shown in Fig. 2a. More comprehensive characterized the SWCNT-modified cloth by SEM is presented in Supporting Information. High magnification SEM images in Fig. 2a (and Fig. S2d and S2f) clearly illustrate uniform deposition of SWCNTs on fabrics, interconnecting the gaps between the fibres. This obviously establishes sufficient electrical conductivity of the resulting material. Indeed, although the thickness of the cloth increased just slightly, from 274 to 292 μm, after SWCNT incorporation, the composite fibres display remarkably good electrical conductivity (Table S1). The textile is originally insulating whereas SWCNT-modified cloth is conductive with its conductivity of 1868 mS $cm^{-1}$ being in the range of previously reported carbon modified textiles. E.g., reported materials include Ketjen carbon black/textile (27 mS $cm^{-1}$), multi-walled CNT (MWCNT)/textile (38 mS $cm^{-1}$), SWCNT/textile (194 mS $cm^{-1}$), MWCNT/SWCNT/textile (194 mS $cm^{-1}$) (Ogawa et al., 2015), and 5–125 S $cm^{-1}$ for SWCNTs/cotton by Hu et al., (2010). Important is that the conductivity of our SWCNT modified cloth was sufficient for biosensor performance; this is supported by experimental data presented below.

It is worth mentioning that the prepared electrode material had specific capacitance of 53 F $g^{-1}$ deduced from CVs at 5 mV $s^{-1}$. Original data and calculations are presented in Supporting Information. Even at increased scan rates (100 mV $s^{-1}$) the SWCNT-modified textile still maintained 36.8 F $g^{-1}$, revealing its sufficient capacitance retention of 69%. This, additionally, suggests that the SWCNT-modified cloth electrode can be rapidly charged and discharged even at high scan rate; the feature may be attributed to good ionic accessibility to the entire surface area of the textile (Yu et al., 2014). The specific capacitance of the SWCNT-modified textile was comparable to recently reported fabric-based electrodes, for example, graphene/cotton composite (40 F $g^{-1}$ at 5 mV $s^{-1}$) (Xu et al., 2015), N/O-enriched carbon microfibers cloth (2.4 F $cm^{-2}$ at 1.0 mA $cm^{-2}$) (Qin et al., 2017), SWCNTs/cotton (80 F $g^{-1}$ at 1.0 mA $cm^{-2}$) (Hu et al., 2010), double-walled CNTs/bacterial nanocellulose papers (46.9 F $g^{-1}$ at 100 mV $s^{-1}$) (Kang et al., 2012), graphene nanosheet/cotton (81.7 F $g^{-1}$ at 10 mV $s^{-1}$) (Liu et al., 2012), SWCNT film (36 F $g^{-1}$ at 1.0 mA $cm^{-2}$) (Kaempgen et al., 2009) and 3D microporous graphene film (58 F $g^{-1}$ at 1.0 A $g^{-1}$) (Chen et al., 2012).

The electrode area (electrochemically assessable geometric area) was determined from CVs with ferricyanide/ferrocyanide redox couple. The CVs and calculations are presented in Supplementary Information. It was found that the electrode area is equal to 2.26 $cm^2$, which is close to approximately estimated 2 $cm^2$ geometric area of the cloth electrode

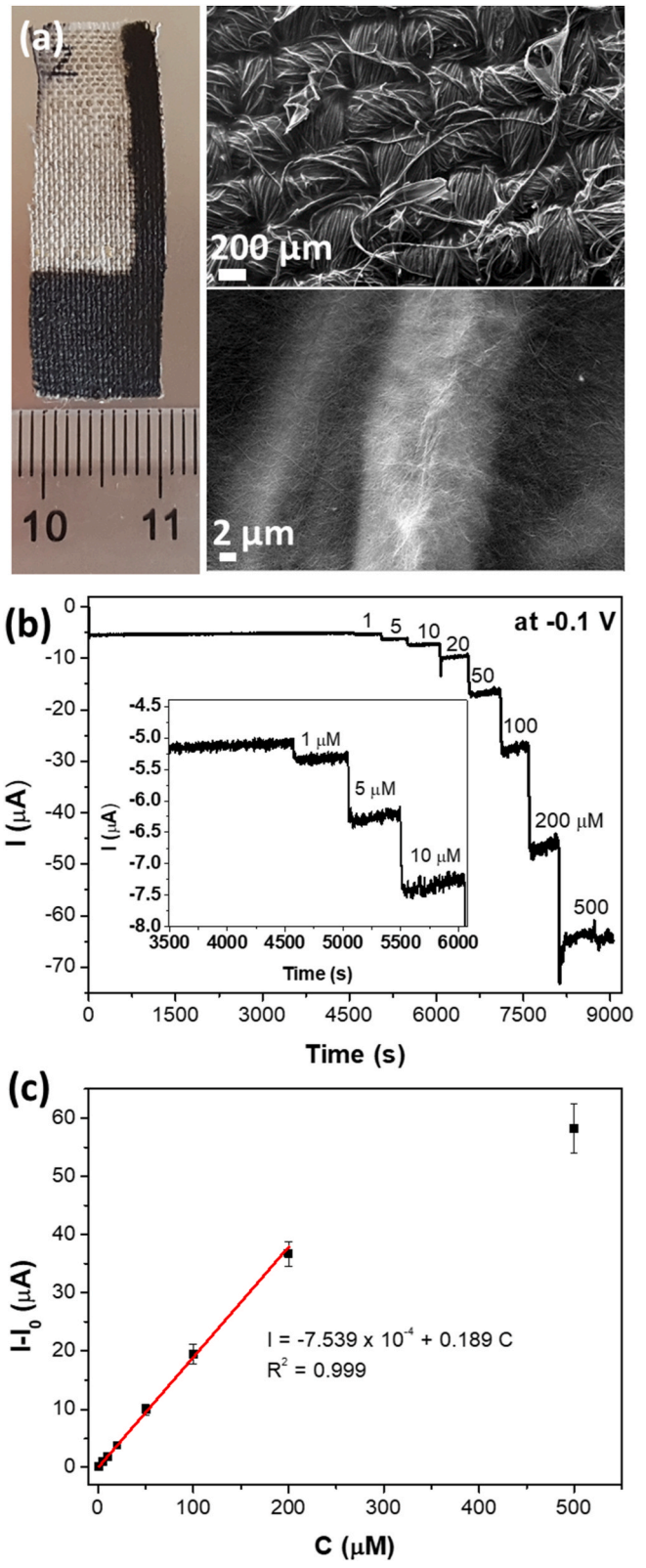


**Fig. 2.** (a) Photo and SEM images of SWCNT-modified cloth electrode. (b) Amperometric *i-t* curve of HRP/SWCNT-modified cloth in a PBS electrolyte (pH 7.4) with successive addition of $H_2O_2$ (1–500 µM). The inset shows the enlarged response with successive addition of $H_2O_2$ at low concentrations (1–10 µM). (c) The plot, steady-state current change vs concentration, represent a calibration plot derived from the data in (b). $I_0$ is electrode current before addition of $H_2O_2$ into the measurement cell. The error bars indicate a standard deviation of measured data of three independently prepared electrodes.

(the values account ferro-/ferricyanide diffusion from both sides of 1 $cm^2$ electrode). The interfacial and electrochemical characteristics determined and discussed above indicate that the conducting textile produced by the modification of cloth with SWCNTs should be well-sufficient as an electrode material for making $H_2O_2$ biosensor. Specifically, the characteristics discussed above indicate that the biosensor will not be limited by the textile conductivity since the currents generated by the biosensor signal response are expected to be low.

### 3.2. Characterization of $H_2O_2$ biosensor based in textile electrode

To convert the textile electrode into a $H_2O_2$ electrochemical biosensor, we immobilized horseradish peroxidase (HRP) enzyme on the surface of SWCNT-modified cloth. The successful immobilization and establishment of direct electron transfer contact between HRP and the surface of the SWCNT-modified textile electrode was confirmed by OCP measurements of the electrodes. The OCP value of the HRP/SWCNT-modified textile electrode was found to be equal to 0.54 V (vs Ag/AgCl) compared to 0.28 V of HRP-free SWCNT-modified textile electrode (Fig S8, Supporting Information). The results showed that the OCP value of the HRP/SWCNT-modified textile electrode became closer to the potential range of 0.63–0.69 V (vs SCE) known for redox transitions of Compounds I/HRP and Compound I/Compound II, as indicated by reactions 2–4 (Dequaire et al., 2002; Nandini et al., 2013; Razumas et al., 1992; Ruzgas et al., 1996). The detected shift of the OCP towards the values of the redox potentials of Compounds I/HRP and Compound I/Compound II, thus, indicates the establishment of efficient direct electron coupling between the HRP and the surface of SWCNT-modified textile electrode, where the redox reactions 2–4 determine the potential of the electrode.

$$HRP(Fe^{3+}) + H_2O_2 \rightarrow \text{Compound I } ([Fe^{4+}{=}O]^{\bullet+}) + H_2O \quad (2)$$

$$\text{Compound I } ([Fe^{4+}{=}O]^{\bullet+}) + e^- + H^+ \rightarrow \text{Compound II } (Fe^{4+}{=}O) \quad (3)$$

$$\text{Compound II } (Fe^{4+}{=}O) + e^- + H^+ \rightarrow HRP(Fe^{3+}) + H_2O \quad (4)$$

Next, the electrochemical biosensing ability was investigated by recording current response of the HRP/SWCNT-modified textile electrode to $H_2O_2$ at an applied voltage of −0.1 V; this applied potential is regarded as optimal for amperometric biosensors based on direct electron transfer of HRP (Ruzgas et al., 1996). Fig. 2b represents a typical amperometric response for consecutive additions of different concentrations of $H_2O_2$ (1–500 µM) to PBS. The HRP/SWCNT-modified textile shows a quick response (within 6 s to reach >90% maximum steady-state current). The corresponding calibration curve is illustrated in Fig. 2c. The calibration curve was fitted to an electrochemical Michaelis-Menten equation (equation (5)) giving estimates for maximal current, $I_{max}$, and apparent Michaelis constant, $K_{m,app}$, of 160 µA and 0.78 mM, respectively.

$$I = \frac{I_{max} \cdot c}{K_{m,app} + c} \quad (5)$$

where $I$ is a registered electrode current response ($I$–$I_0$ in Fig. 2c) at certain $H_2O_2$ concentration, $c$.

The $I_{max}$ and $K_{m,app}$ values indicate that the biosensor has a sufficient linear range; it is expected that ROS generated $H_2O_2$ concentration on skin will usually be far below 1 mM (Jankovskaja et al., 2020). The initial part of the calibration curve can be regarded as linear in the range of 1–200 µM: $\Delta I(I–I_0, \mu A) = -7.539 \times 10^{-4} + 0.189$ x C (µM) with a square of correlation coefficient $r^2 = 0.999$ (n = 7). $I_0$ is electrode current before addition of $H_2O_2$. Moreover, based on a signal-to-noise ratio of 3 (S/N = 3), the limit of detection (LOD) of the enzyme sensor is estimated to be 0.3 µM $H_2O_2$ while the sensitivity of the enzyme-modified electrode is 184 µA $mM^{-1}$ $cm^{-2}$. The biosensor characteristics compares well with the analytical performance of previously reported $H_2O_2$ biosensors based on HRP enzyme (see Table S2). The

sensitivity to $H_2O_2$ could be, however, future improved since it is lower than the estimate of $H_2O_2$ diffusion limited sensitivity of approximately 1 A $M^{-1}$ $cm^{-2}$ (Ruzgas et al., 1996).

### 3.3. Performance of the $H_2O_2$ biosensor in Franz cell: amperometric measurements

To demonstrate possible application of Franz cells in biosensor research, the $H_2O_2$ biosensor electrode was placed into a Franz cell as shown in Fig. 1. It should be mentioned that the proposed configuration of reference and counter electrodes is one of the simplest. However, it could be imagined that all three electrodes could have been printed on the cloth and thus could be placed directly on the skin or dialysis membrane in the upper chamber of the Franz cell. The shown electrode configuration might be advantageous at the stage when the research is focused on the optimization of biosensor transduction reactions, choice of materials and biosensor preparation protocols, i.e., when the focus of the work is on optimization of the working electrode and its interface with the skin. Below the performance of HRP/SWCNT-modified textile electrode in the Franz cell for determining $H_2O_2$ is described.

The $H_2O_2$ was pipetted into the lower chamber of the Franz cell and amperometric response to $H_2O_2$ was recorded with the biosensor in the upper chamber of the Franz cell. It is clear that the amperometric response (Fig. 3) is due to the penetration of $H_2O_2$ through a dialysis or skin membrane, which separates the upper and the lower chambers of the Franz cell. In the case of skin surrogate, dialysis membrane, and the injection of 0.5 mM of $H_2O_2$ into the lower chamber, the concentration of permeated $H_2O_2$ (examined via the calibration plot, Fig. 2c) was 11.58 ± 2.51 μM. The HRP/SWCNT-modified textile shows a response time of 180 s to reach 90% maximum steady-state current after 0.5 mM $H_2O_2$ addition to the lower chamber of the Franz cell.

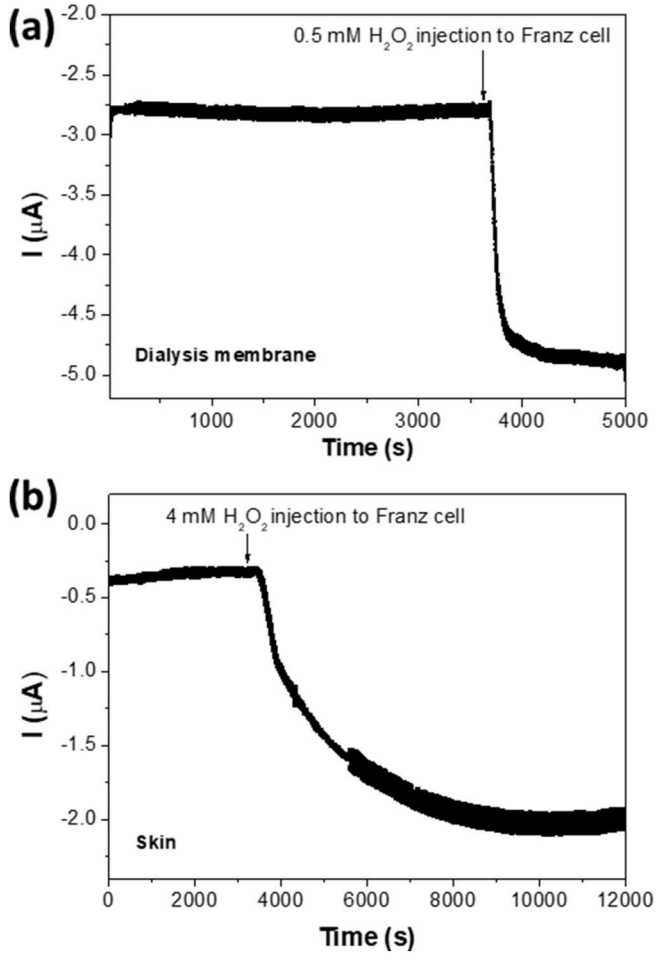


**Fig. 3.** Amperometric *i-t* curve recorded with HRP/SWCNT-modified cloth electrode placed on top of (a) dialysis and (b) skin membrane in the Franz cell as shown in Fig. 1. The applied voltage was −0.1 V vs. Ag/AgCl/KClsat. In (a) 0.5 mM $H_2O_2$ was injected in to the lower chamber of the Franz cell filled with PBS, dialysis membrane was used as skin surrogate. In (b) 4 mM $H_2O_2$ was injected in to the lower chamber of the Franz cell containing PBS electrolyte. To inactivate catalase present in skin, the skin membrane was UVB-irradiated for 5 h before placing it in to the Franz cell.

In the next experiment, the dialysis membrane was replaced by a skin membrane with a thickness of 500 μm. It should be emphasized that no current response to $H_2O_2$ addition in the lower chamber of the Franz cell was possible to record with the HRP/SWCNT-modified electrode in this experiment. The problem is that skin has highly active catalase which efficiently converts penetrating $H_2O_2$ into $H_2O$ and $O_2$ prior the $H_2O_2$ reaches HRP/SWCNT-modified textile electrode. High catalase activity in skin as well as in other biological barriers is well documented (Hernández et al., 2019; Rajendran et al., 2021). Thus, to continue the planned $H_2O_2$ biosensor studies in Franz cell the catalase in skin must be inhibited by irreversible inhibitors or bleaching by prolonged UV-irradiation of skin. The use of inhibitors is not straightforward because the same inhibitors usually inhibit also HRP, i.e., the enzyme biosensor. We chose to bleach catalase by 5-h UVB-irradiation before putting it to the Franz cell. This treatment might also be problematic due to the risk to affect permeability through skin. The UVB effect on the skin was previously studied and the deterioration of barrier properties was noticed only in case of skin UVB irradiation in the presence of an oxidant such as $H_2O_2$ (Hernandez et al., 2019). However, even keeping in mind this possibility of increased permeability through skin after the 5-h UVB-based inactivation of the catalase, it was not possible to observe the biosensor response to 0.5 mM of $H_2O_2$ injected into the lower chamber (data not shown). When the concentration of $H_2O_2$ in the lower chamber was increased to 4 mM, the permeable $H_2O_2$ was recorded reaching concentration of 9.66 ± 0.19 μM (Fig. 3b). As it can be seen in Fig. 3b, the *invitro* biosensor illustrates that the diffusion of the $H_2O_2$ through skin is very slow (takes approximately 2 h to reach steady-state current). It was previously shown that the tough diffusional barrier for penetration of hydrophilic solutes such as $H_2O_2$ and glucose is represented by stratum corneum part of the skin (Nocchi et al., 2017; Ullah et al., 2018). In this context, it can be mentioned that penetration of metabolites through stratum corneum might be quicker in the case of higher abundance of hair follicles in skin (Jankovskaja et al., 2020).

The results presented and discussed above clearly demonstrate that the studies of biosensors in Franz cell setup offer a number of additional opportunities, which are not possible in *in vivo* experiments. In this particular work, we demonstrate that activity of enzymes in skin can severely influence the expected biosensor responses. It should be mentioned that effects of skin enzymes and microbiota in epidermal biosensor developments are seldom considered. Though, microbiota dependent degradation of metabolites (e.g., amino acids) penetrating the skin is expected and has been previously demonstrated (Jankovskaja et al., 2021).

### 3.4. Performance of the $H_2O_2$ biosensor in Franz cell: wireless measurement

To demonstrate a possibility to use Franz cell setup for studies of wireless biosensors we adopted the chip-less, battery-less biosensor tag antenna design reported previously (Larpant et al., 2019). The biosensor tag design comprised three important components, Fig. 4a. Specifically, (i) antenna of a NFC tag, (ii) screen printed electrode (SPE), and (iii) HRP/SWCNT-modified textile electrode. As shown in Fig. 4a, the SPE was coupled into the antenna circuit by removing 5 mm of the antenna metal line and connecting the ends of the broken antenna to the working and the counter electrodes of the SPE. To realize electrical conductivity of the antenna circuit, of this antenna-SPE connection, a layer of AgNPs

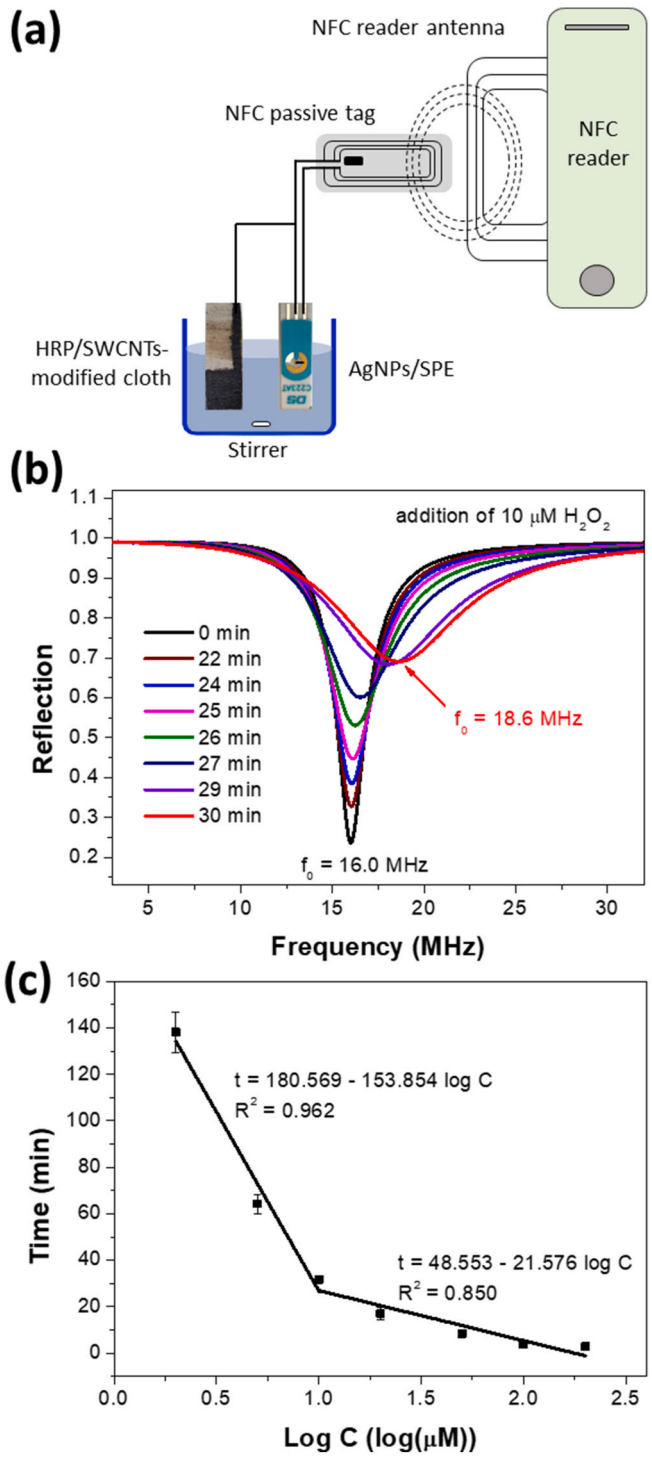


**Fig. 4.** The illustration of the coupling of (a) tag antenna and SPE (containing AgNP layer) to a textile biosensor for wireless measurements of $H_2O_2$ concentration in PBS. The biosensor was based on textile comprised of HRP/SWCNT-modified cloth. The tag was NFC tag where the tag antenna was broken and reconnected with an AgNP layer placed on the SPE connected to the tag. (b) The electromagnetic field reflection response (S11 characteristic), measured with the tag before (curve corresponding to characteristic frequency of 16 MHz) and after addition of 10 μM $H_2O_2$ to a PBS. Different curves demonstrate transition of S11 in time after addition of the $H_2O_2$ into the measurement cell. (c) The relationship between the response time (time needed for characteristic frequency of the tag to shift from 16 MHz to 18.6 MHz) and $H_2O_2$ concentration. The electrode connections and conditions are the same as in (a) and (b), respectively. The error bars indicate a standard deviation of measured data of three repeated measurements.

was deposited between the working and the counter electrodes on the SPE. This layer, in principle, repairs broken tag antenna circuit since the deposited AgNP layer is highly conducting. As shown in Fig. 4a, the HRP/SWCNT-modified electrode was connected to the working electrode of the SPE. This, HRP/SWCNT-modified electrode connection to an AgNP layer enables wireless $H_2O_2$ sensing; HRP/SWCNT-modified electrode functions as sensing biocathode. Specifically, the essence of the detection mechanism is that in the presence of $H_2O_2$ the HRP/SWCNT-modified electrode performs electroreduction of $H_2O_2$ by oxidising AgNP layer to AgCl. This process converts highly conducting AgNP layer to practically non-conducting AgCl layer. Since the AgNP layer is a part of the antenna circuit the Ag/AgCl transition can be wirelessly detected. It should be mentioned that the AgNP conversion to AgCl can be examined by measurements of AgNP layer resistance (the setup and experimental results are described in Supporting Information, and Fig. S7).

The HRP/SWCNT-modified electrode (biocathode) driven Ag/AgCl redox transition in the AgNP layer, in the tag antenna-SPE setup, can be read by the tag antenna reader, specifically, vector network analyzer (VNA). The use of VNA allows excitation of the tag antenna by the VNA antenna at different frequencies, e.g., by radio frequency scanning from 5 to 100 MHz. At the same time, during this frequency scan, the VNA measures an electromagnetic power which is absorbed by closely placed biosensor tag antenna. It is relevant to note that the intact tag, used in our studies, had maximum absorbtion of electromagnetic energy at 13.56 MHz. The dependence of the fraction of the adsorbed power on the frequency of the excitation field, generated by VNA antenna, is usually presented by a reflection plot, S11, as shown in Fig. 4b. The frequency at which the absorption is maximal, i.e., at the minimum of S11 reflection curve, is called characteristic or resonance frequency of the tag. In our tag antenna-SPE system, the characteristic frequency above 17 MHz, e.g., 18.6 MHz was found for the case when the AgNP layer was in a state of AgCl, Fig. 4b. The tag antenna-SPE system with AgNP layer comprised of metallic Ag showed characteristic frequency below 17 MHz, specifically, 16 MHz in Fig. 4b. Fig. 4b also demonstrates the S11 curves at different times after the addition of 10 μM $H_2O_2$ into the measurement cell shown in Fig. 4a. The S11 curves, initially, characterized by characteristic frequency of 16 MHz transit to the S11 curve with the characteristic frequency of 18.6 MHz. The observed transition clearly demonstrates that $H_2O_2$ can be detected wirelessly by the described biosensor tag comprised of the tag antenna, SPE containing AgNP layer and the HRP/SWCNT-modified e-textile electrode.

As shown in Fig. 4b, after 10 μM $H_2O_2$ was added into the measurement cell containing HRP/SWCNT-modified textile electrode and the SPE with AgNP layer (Fig. 4a), the tag characteristic frequency shifted from 16.0 to 18.6 MHz (Fig. 4b). The frequency transition was not immediate and required 31.7 ± 0.7 min at 10 μM $H_2O_2$. It was previously proven that the response time, i.e., the time needed to convert deposited AgNPs to AgCl depended on the amount of electricity, i.e., the current generated by the $H_2O_2$ biosensor, and, thus, on $H_2O_2$ concentration (Larpant et al., 2019). The relationship between the response time of the biosensor tag and $H_2O_2$ concentration is shown in semi-logarithmic coordinates in Fig. 4c (the values are presented in Table S3). These results suggest successful development of chip-less, battery-less and contactless $H_2O_2$ biosensor based on Ag/AgCl redox conversion driven by $H_2O_2$ electroreduction at HRP/SWCNT-modified textile electrode.

For demonstration of the versatility of Franz cell setup, a wireless biosensor described above (Fig. 4a) was placed into the upper chamber of the Franz cell while leaving the tag antenna free from contact with the solution (Fig. 5a). For these experiments, $H_2O_2$ permeability through skin surrogate, dialysis membrane, separating the upper and lower chamber of the cell, was first examined. The lower chamber was filled with 6 mL PBS and the upper chamber with 0.6 mL PBS. The wireless measurements of S11 function (reflection) showed that the battery-less and wireless biosensor in the Franz cell had characteristic frequency

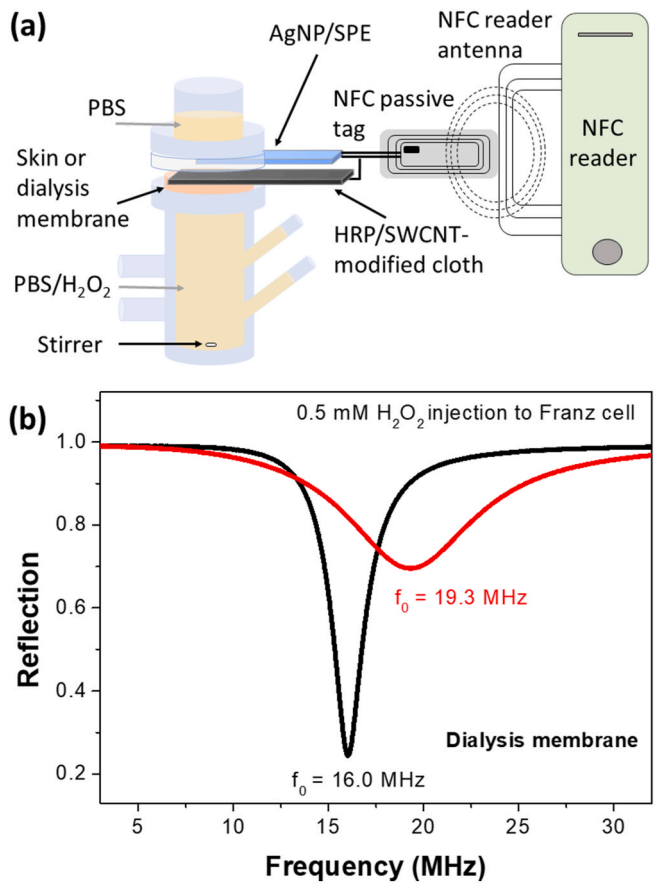


**Fig. 5.** (a) Franz cell equipped with HRP/SWCNT-modified textile electrode for chip-less and battery-less wireless measurements of $H_2O_2$, which penetrates skin membrane or its model, dialysis membrane. The cell consists of two chambers, which are separated by skin or its model dialysis membrane. The upper chamber is filled with buffer and host working, HRP/SWCNT-modified cloth based $H_2O_2$ sensing, electrode. The upper chamber also hosts a SPE electrode (AgNP/SPE), which integrates an AgNP layer into an antenna circuit of a passive NFC tag. The lower chamber is filled with the PBS, which is agitated by magnetic stirrer. The analyte of interest, particularly, $H_2O_2$ is added to the lower chamber, which penetrates the membrane and is wirelessly registered with the $H_2O_2$ biosensor tag antenna. The setup mimics electrochemical monitoring of $H_2O_2$, which might be generated in viable tissue, e.g., during infection or inflammation; (b) The reflection response (S11) before (black line with $f_0$ of 16 MHz) and after addition of 0.5 mM $H_2O_2$ to the lower chamber of a Franz cell containing PBS (pH 7.4). S11 trace (red line) with $f_0$ of 19.3 MHz was obtained in the end of the experiment, when AgNP layer on the SPE electrode was electrooxidized to AgCl by $H_2O_2$ electroreduction on HRP/SWCNT-modified electrode. The S11 traces were obtained with the setup shown in (a) and dialysis membrane separating upper and lower chambers of the Franz cell. (For interpretation of the references to colour in this figure legend, the reader is referred to the Web version of this article.)

of 16 MHz as expected for the case of the AgNP layer connected into the antenna by the SPE. The response of the biosensor to addition of 0.5 mM of $H_2O_2$ into the lower chamber was wirelessly recorded by registering S11 curves (Fig. 5b). The response time for the characteristic frequency change, determined from the reflection vs frequency plot (Fig. 5b) was estimated to be equal to 27.7 ± 0.3 min. According to the calibration plot presented in Fig. 4b, this corresponded to 9.86 ± 0.05 μM $H_2O_2$ in the receptor chamber. The determined concentration is very similar to the concentration of $H_2O_2$ detected in similar amperometric experiment presented in Fig. 3a, which confirms the validity of the wireless $H_2O_2$ measurement.

Similar experiments, through introducing 4 mM of $H_2O_2$, have been repeated with skin membrane in the Franz cell. Wireless response was possible to observe, however, the response time needed for the transition of the characteristic frequency of the tag coupled to AgNP/SPE and HRP/SWCNTs-modified textile was longer than 1 h (see Fig S6, Supporting Information) as well as irreproducible for each new skin membrane which we tested. The irreproducibility can be caused by the differences of catalase activity in skin and its inactivation by UVB irradiation. Biological variability of skin diffusional barrier to $H_2O_2$ permeability obviously is another problem. How to deal with these biological issues in studies of epidermal biosensors will be an objective of our future research. Nevertheless, the experiments with Franz cells are extremely useful in addressing a considerable number of biosensor development issue. The system allows to test biosensor concepts using skin surrogates as well as clearly indicates a number of issues when real biological skin membranes are used. These examples of problems are often neglected or hidden in experiments of direct testing of epidermal biosensors on animals or humans. Thus, broader use of Franz cell in development of biosensors might be beneficial to learn and address the obstacles of, e.g., epidermal sensing before going for biosensor testing on animals. Current progress in producing skin equivalents from cell cultures will definitely provide a number of animal free experimental alternatives which in the future might increase versatility and usefulness of Franz cell based setup in biosensor and bioelectronics research.

## 4. Conclusions

Reducing animal use in biosensor research requires broader use of *in vitro* methods. Epidermal biosensing, including an exploding research area on wearables, could benefit from *in vitro* methods and techniques developed and validated in the relevant research area of topical and transdermal drug delivery. In this work, we demonstrate novel application of Franz cell setup in biosensor research. We show how Franz cell setup can be equipped with different electrodes enabling development and characterization of biosensors, which are intended for functioning in close proximity to skin. A chosen example was a $H_2O_2$ biosensor based on HRP/SWCNT-modified textile. The obtained HRP/SWCNT-modified textile electrode showed a lower detection limit of 0.3 μM, linear calibration up to 200 μM, and sensitivity of 184 μA $mM^{-1}$ $cm^{-2}$. The biosensor was placed in close proximity to skin membrane or skin surrogate, dialysis membrane, in the Franz cell setup. The biosensor, in amperometric mode, was able to monitor penetration of $H_2O_2$ through skin and dialysis membrane. The analysis of the data revealed that the catalase activity in the skin is a considerable problem in studies of $H_2O_2$ detection at skin surface. The activity of this enzyme in skin should obviously be considered if epidermal biosensor targets $H_2O_2$ registration, i.e., topical ROS detection. The Franz cell experiments clearly present opportunities for studies of biosensor-skin interface which are more difficult to address by *in vivo* experiments in animals or humans, e.g., inhibition of some enzymes in skin might not be possible in *in vivo* settings. Subsequently, a chip-less and battery-less, contactless biosensor was also fabricated to demonstrate that even wireless biosensor system could be studied by using Franz cell setup. In general, we present, Franz cell setup, which is not yet explored in development of epidermal and wearable biosensors. We think that the setup should be beneficial for reducing the use of animals in biosensor research.

## CRediT authorship contribution statement

**Van Chinh Hoang:** Data curation, Writing – original draft, made the main body of experiments, processed data and wrote the first draft of the manuscript. **Atefeh Shafaat:** Writing – review & editing, conducted initial wireless measurements with the biosensors, synthesised AgNPs and conducted DLS measurements, edited the manuscript. **Skaidre Jankovskaja:** Supervision, Writing – review & editing, initial Franz cell experiments, prepared skin membranes, edited the manuscript. **Vincent G. Gomes:** Writing – review & editing, Conceptualization, conducted conceptualization of the work, performed final editing of the

manuscript. **Tautgirdas Ruzgas:** Conceptualization, Supervision, Writing – review & editing, conducted conceptualization and supervision of the work, performed final editing of the manuscript.

## Declaration of competing interest

The authors declare that they have no known competing financial interests or personal relationships that could have appeared to influence the work reported in this paper.

## Acknowledgements

V.C. Hoang is grateful to the University of Sydney for an International Postgraduate Research Scholarship. Financial support from the Knowledge Foundation (20170058 and 20190010), the Swedish Research Council (2018–04320) and the Biofilms - Research Center for Biointerfaces at Malmö University are gratefully acknowledged. TR thank the Gustaf Th. Ohlsson Foundation. The authors also acknowledge Mr. Maxim Morin at Malmö University for his assistance with skin preparation.

## Appendix A. Supplementary data

Supplementary data to this article can be found online at https://doi.org/10.1016/j.bios.2021.113420.

## References

Bandodkar, A.J., Jia, W., Wang, J., 2015. Electroanalysis 27 (3), 562–572.
Bartosova, L., Bajgar, J., 2012. Curr. Med. Chem. 19 (27), 4671–4677.
Bjoerklund, S., Ruzgas, T., Nowacka, A., Dahi, I., Topgaard, D., Sparr, E., Engblom, J., 2013. Biophys. J. 104 (12), 2639–2650.
Chen, C.-M., Zhang, Q., Huang, C.-H., Zhao, X.-C., Zhang, B.-S., Kong, Q.-Q., Wang, M.-Z., Yang, Y.-G., Cai, R., Sheng Su, D., 2012. Chem. Commun. 48 (57), 7149–7151.
Dequaire, M., Limoges, B., Moiroux, J., Savéant, J.-M., 2002. J. Am. Chem. Soc. 124 (2), 240–253.
Goh, K., Setiawan, L., Wei, L., Jiang, W., Wang, R., Chen, Y., 2013. J. Membr. Sci. 446, 244–254.
Guy, R.H., Kalia, Y.N., Delgado-Charro, M.B., Merino, V., Lopez, A., Marro, D., 2000. J. Contr. Release 64 (1–3), 129–132.
Heikenfeld, J., 2016. Nature (London, U. K.) 529 (7587), 475–476.
Heikenfeld, J., Jajack, A., Rogers, J., Gutruf, P., Tian, L., Pan, T., Li, R., Khine, M., Kim, J., Wang, J., Kim, J., 2018. Lab Chip 18 (2), 217–248.
Hernández, A.R., Boutonnet, M., Svensson, B., Butler, E., Lood, R., Blom, K., Vallejo, B., Anderson, C., Engblom, J., Ruzgas, T., Björklund, S., 2019. J. Contr. Release 306, 121–129.
Hernandez, A.R., Vallejo, B., Ruzgas, T., Bjorklund, S., 2019. Sensors 19 (10), 2376.
Hu, L., Pasta, M., La Mantia, F., Cui, L., Jeong, S., Deshazer, H.D., Choi, J.W., Han, S.M., Cui, Y., 2010. Nano Lett. 10 (2), 708–714.
Jankovskaja, S., Engblom, J., Rezeli, M., Marko-Varga, G., Ruzgas, T., Bjoerklund, S., 2021. Sci. Rep. 11 (1), 678.
Jankovskaja, S., Engblom, J., Ruzgas, T., Jankovskaja, S., Engblom, J., Ruzgas, T., Labrousse, A., Prevaud, L., Holmqvist, B., Brinte, A., Rezeli, M., Marko-Varga, G., 2020. Mikrochim. Acta 187 (12), 656.
Junqueira Garcia, M.T., Lopes de Vasconcellos, F.L., Raffier, C.P., Roberts, M.S., Grice, J. E., Elizabeth Benson, H.A., Leite-Silva, V.R., 2018. Curr. Top. Med. Chem. 18 (4), 287–299.
Kaempgen, M., Chan, C.K., Ma, J., Cui, Y., Gruner, G., 2009. Nano Lett. 9 (5), 1872–1876.
Kang, Y.J., Chun, S.-J., Lee, S.-S., Kim, B.-Y., Kim, J.H., Chung, H., Lee, S.-Y., Kim, W., 2012. ACS Nano 6 (7), 6400–6406.
Keum, D.H., Kim, S.-K., Koo, J., Lee, G.-H., Jeon, C., Mok, J.W., Mun, B.H., Lee, K.J., Kamrani, E., Joo, C.-K., Shin, S., Sim, J.-Y., Myung, D., Yun, S.H., Bao, Z., Hahn, S.K., 2020. Sci. Adv. 6 (17) eaba3252.
Larpant, N., Pham, A.D., Shafaat, A., Gonzalez-Martinez, J.F., Sotres, J., Sjoholm, J., Laiwattanapaisal, W., Faridbod, F., Ganjali, M.R., Arnebrant, T., Ruzgas, T., 2019. Sci. Rep. 9 (1), 12948.
Liu, W.-w., Yan, X.-b., Lang, J.-w., Peng, C., Xue, Q.-j., 2012. J. Mater. Chem. 22 (33), 17245–17253.
Mitragotri, S., 2003. J. Contr. Release 86 (1), 69–92.
Morin, M., Ruzgas, T., Svedenhag, P., Anderson, C.D., Ollmar, S., Engblom, J., Bjoerklund, S., 2020. Sci. Rep. 10 (1), 17218.
Nandini, S., Nalini, S., Manjunatha, R., Shanmugam, S., Melo, J.S., Suresh, G.S., 2013. J. Electroanal. Chem. 689, 233–242.
Niehues, H., Zeeuwen, P.L.J.M., van, d.B.E.H., Bouwstra, J.A., El, G.A., Brandner, J.M., 2018. Exp. Dermatol. 27 (5), 501–511.
Nocchi, S., Bjoerklund, S., Svensson, B., Engblom, J., Ruzgas, T., 2017. Biosens. Bioelectron. 93, 9–13.
Ogawa, Y., Takai, Y., Kato, Y., Kai, H., Miyake, T., Nishizawa, M., 2015. Biosens. Bioelectron. 74, 947–952.
Park, S., Jayaraman, S., 2003. MRS Bull. 28 (8), 585–591.
Qin, T., Peng, S., Hao, J., Wen, Y., Wang, Z., Wang, X., He, D., Zhang, J., Hou, J., Cao, G., 2017. Advanced Energy Materials 7 (20).
Rajendran, S.T., Huszno, K., Debowski, G., Sotres, J., Ruzgas, T., Boisen, A., Zor, K., 2021. Bioelectrochemistry 138, 107720.
Raney, S., Lehman, P., Franz, T., 2008. Drug Delivery Technol 8 (7), 32–34, 36-37.
Ray, T.R., Choi, J., Bandodkar, A.J., Krishnan, S., Gutruf, P., Tian, L., Ghaffari, R., Rogers, J.A., 2019. Chem. Rev. 119 (8), 5461–5533.
Razumas, V., Kazlauskaite, J., Ruzgas, T., Kulys, J., 1992. 28(1–2), 159-176.
Ruzgas, T., Csoeregi, E., Emmneus, J., Gorton, L., Marko-Varga, G., 1996. Anal. Chim. Acta 330 (2–3), 123–138.
Salim, A., Lim, S., 2019. Biosens. Bioelectron. 141, 111422.
Schallreuter, K.U., Moore, J., Wood, J.M., Beazley, W.D., Gaze, D.C., Tobin, D.J., Marshall, H.S., Panske, A., Panzig, E., Hibberts, N.A., 1999. J. Invest. Dermatol. Symp. Proc. 4 (1), 91–96.
Stoppa, M., Chiolerio, A., 2014. Sensors 14 (7), 11957–11992.
Stuart, T., Cai, L., Burton, A., Gutruf, P., 2021. Biosens. Bioelectron. 178, 113007.
Taylor, K., Alvarez, L.R., 2019. Altern Lab Anim 47 (5–6), 196–213.
Ullah, S., Hamade, F., Bubniene, U., Engblom, J., Ramanavicius, A., Ramanaviciene, A., Ruzgas, T., 2018. Biosens. Bioelectron. 110, 175–179.
van den Bogaard, E., Ilic, D., Dubrac, S., Tomic-Canic, M., Bouwstra, J., Celli, A., Mauro, T., 2021. J. Invest. Dermatol. 141 (1), 203–205.
Ventura, S.A., Heikenfeld, J., Brooks, T., Esfandiari, L., Boyce, S., Park, Y., Kasting, G.B., 2017. Bioelectrochemistry 114, 54–60.
Wang, S., Oh, J.Y., Xu, J., Tran, H., Bao, Z., 2018. Acc. Chem. Res. 51 (5), 1033–1045.
Xu, K., Lu, Y., Takei, K., 2019. Adv. Mater. Technol. (Weinheim, Ger.) 4 (3) (n/a).
Xu, L.-L., Guo, M.-X., Liu, S., Bian, S.-W., 2015. RSC Adv. 5 (32), 25244–25249.
Yu, D., Goh, K., Wang, H., Wei, L., Jiang, W., Zhang, Q., Dai, L., Chen, Y., 2014. Nat. Nanotechnol. 9 (7), 555–562.